

Intrastriatal Transplantation of Retinal Pigment Epithelial Cells for the Treatment of Parkinson Disease: In Vivo Longitudinal Molecular Imaging with ^{18}F -P3BZA PET/CT¹

Lihong Bu, MD, PhD
Renfei Li, MD, PhD
Hongguang Liu, PhD
Wei Feng, PhD
Xiaoxing Xiong, PhD
Heng Zhao, PhD
Douglas Vollrath, PhD
Baozhong Shen, MD, PhD
Zhen Cheng, PhD

¹From the Molecular Imaging Program at Stanford (MIPS), Department of Radiology and Bio-X Program, Stanford University, 1201 Welch Rd, Lucas Center, Room P095, Stanford, CA 94305-5484 (L.B., R.L., H.L., Z.C.); Molecular Imaging Center, Department of Radiology, The 4th Hospital of Harbin Medical University, Harbin, Heilongjiang, P.R. China (L.B., R.L., B.S.); and Departments of Genetics (W.F., D.V.) and Neurosurgery (X.X., H.Z.), School of Medicine, Stanford University, Stanford, Calif. From the 2013 RSNA Annual Meeting. Received August 29, 2013; revision requested October 9; revision received December 18; accepted January 24, 2014; final version accepted February 7. Supported in part by the Office of Science (BER), U.S. Department of Energy (grant DE-SC0008397), In vivo Cellular Molecular Imaging Center (grant P50 CA114747), Projects of Funds for International Cooperation and Exchange of the National Natural Science Foundation of China (grant 31210103913), and China National Natural Science Funds for Young Scholar (grant 81201125). **Address correspondence to** Z.C. (e-mail: zcheng@stanford.edu).

© RSNA, 2014

Purpose:

To evaluate the performance of *N*-[2-(diethylamino)ethyl]- ^{18}F -5-fluoropicolinamide (^{18}F -P3BZA) for visualizing porcine retinal pigment epithelium (pRPE) cells transplanted in the striatum for the treatment of Parkinson disease and to monitor the long-term activity of implanted pRPE cells by means of ^{18}F -P3BZA positron emission tomography (PET)/computed tomography (CT) in vivo.

Materials and Methods:

Animal work was conducted in accordance with the administrative panel on laboratory animal care. In vitro cell uptake of ^{18}F -P3BZA was determined with incubation of melanotic pRPE or amelanotic ARPE-19 cells with ^{18}F -P3BZA. To visualize the implanted pRPE cells in vivo, normal rats (four per group) were injected with pRPE or ARPE-19 cells attached to gelatin microcarriers in the left striatum and with control gelatin microcarriers in the right striatum and followed up with small animal PET/CT. Longitudinal PET/CT scans were acquired in 12 rats up to 16 days after surgery. Postmortem analysis, which included autoradiography and hematoxylin-eosin, Fontana-Masson, and immunofluorescence staining, was performed. Data were compared with the Student *t* test, analysis of variance, and regression analysis.

Results:

^{18}F -P3BZA accumulated in pRPE cells effectively (3.48% of the injected dose [ID] per gram of brain tissue \pm 0.58 at 1 hour after injection of the probe at 2 days after surgery in vivo) but not in control ARPE-19 cells ($P < .05$). Longitudinal PET/CT scans revealed that the activity of implanted pRPE cells decreased over time, as evidenced by a reduction in ^{18}F -P3BZA uptake (3.39% ID/g \pm 0.18, 2.49% ID/g \pm 0.41, and 1.20% ID/g \pm 0.13 at days 2, 9, and 16, respectively; $P < .05$). Postmortem analysis helped confirm the results of in vivo imaging.

Conclusion:

^{18}F -P3BZA PET/CT is a feasible technique for visualizing and detecting the activity of implanted RPE cells in vivo.

© RSNA, 2014

Online supplemental material is available for this article.

Parkinson disease is a neurodegenerative disorder with a selective vulnerability of dopaminergic neurons in the substantia nigra pars compacta, which shows irreversible loss of dopamine in the striatum as a consequence. Parkinson disease affects

approximately 1%–2% of the population older than 60 years (1). Striatal transplantation of cells that produce dopamine or L-3,4-dihydroxyphenylalanine (L-DOPA) has been actively investigated for Parkinson disease treatment in preclinical and clinical trials. This treatment has the potential advantage of providing a long-term, continuous dopaminergic source and avoiding motor complications because of the fluctuations and chronic intermittent dopaminergic stimulation associated with oral L-DOPA administration (2–5).

Retinal pigment epithelium (RPE) cells accumulate L-DOPA as a precursor for the formation of their characteristic melanin pigment (6). Apart from L-DOPA production, human RPE (hRPE) cells can also produce a small amount of dopamine directly and possess other molecular machinery involved in dopamine production and regulation (7–10). Therefore, hRPE cells attached to gelatin microcarriers have been explored as a promising source of donor cells for neural transplantation in the treatment of Parkinson disease by providing “L-DOPA pumps” to maintain stable L-DOPA levels (11). Both preclinical studies (in rodents and non-human primates) (12,13) and clinical trials (14,15) indicated that implantation of hRPE cells attached to gelatin microcarriers into the striatum could ameliorate the behavioral deficits of the recipients. However, in another large-scale, multicenter, randomized controlled phase II clinical trial, clinical benefits of this therapy were not observed (16). These discrepant results raise a number of critical issues that must be addressed before further clinical trials are performed. The fact that “no assay is available to detect the activity of hRPE cells following their implantation into the host brain in vivo”

(17) is a major limitation of the studies to date (13,18).

Considering the melanogenesis mechanism of RPE cells for neural transplantation (19,20), we hypothesized that the melanin-targeted small molecule probe *N*-[2-(diethylamino)ethyl]-¹⁸F-5-fluoropicolinamide (¹⁸F-P3BZA) could serve as a positron emission tomography (PET) probe for monitoring RPE cells transplanted into the striatum. The aims of this study were to (a) evaluate the performance of ¹⁸F-P3BZA for visualizing the activity of RPE cells in vivo by monitoring the activity of the melanin and (b) monitor the long-term graft activity of implanted RPE cells following their implantation into the host striatum in vivo by means of ¹⁸F-P3BZA PET/computed tomography (CT).

Advances in Knowledge

- The melanin-targeted PET probe *N*-[2-(diethylamino)ethyl]-¹⁸F-5-fluoropicolinamide (¹⁸F-P3BZA) shows high accumulation in porcine retinal pigment epithelium (pRPE) cells (10.72% ± 0.38 of applied activity within 30 minutes after co-incubation) and excellent imaging contrast (as evidenced by a much higher microcarrier-bound pRPE cells-to-control gelatin microcarriers uptake ratio than microcarrier-bound ARPE-19-cell-to-gelatin microcarriers uptake ratio [3.05 ± 0.57 vs 1.21 ± 0.36, respectively; *P* = .04]).
- ¹⁸F-P3BZA identifies and binds to transplanted pRPE cells specifically in a melanin-dependent manner, as evidenced by the high correlation (*R*² = 0.91) between the ¹⁸F-P3BZA uptake and the melanin content in pRPE cells at different passages and the consistency between the longitudinal PET imaging results and the corresponding postmortem analysis.
- In vivo ¹⁸F-P3BZA PET reveals that the activity of implanted pRPE cells decreases over time after their implantation into the rat brain.
- ¹⁸F-P3BZA shows favorable pharmacokinetics in normal rat brain (the uptakes of ¹⁸F-P3BZA in rat brain are 7.61% of the injected dose [ID] per gram of tissue ± 0.30, 3.54% ID/g ± 0.21, and 1.04% ID/g ± 0.37 at 2, 28, and 60 minutes after injection, respectively), which makes it suitable for targeted imaging of retinal pigment epithelium cells in brain.


Implication for Patient Care

- The melanin-targeted PET probe ¹⁸F-P3BZA provides a promising technique for imaging the activity of retinal pigment epithelium cells implanted for the treatment of patients with Parkinson disease and is worthy of further evaluation in the clinic.

Materials and Methods

Z.C. and L.B. have a patent pending for ¹⁸F-P3BZA. All animal work was conducted in accordance with the

Published online before print

10.1148/radiol.14132042 Content code: 

Radiology 2014; 272:174–183

Abbreviations:

¹⁸F-P3BZA = *N*-[2-(diethylamino)ethyl]-¹⁸F-5-fluoropicolinamide
 hRPE = human RPE
 ID = injected dose
 L-DOPA = L-3,4-dihydroxyphenylalanine
 pRPE = porcine RPE
 RPE = retinal pigment epithelium

Author contributions:

Guarantors of integrity of entire study, L.B., R.L., H.L., B.S., Z.C.; study concepts/study design or data acquisition or data analysis/interpretation, all authors; manuscript drafting or manuscript revision for important intellectual content, all authors; approval of final version of submitted manuscript, all authors; literature research, L.B., R.L., D.V., Z.C.; experimental studies, L.B., R.L., H.L., W.F., X.X., H.Z.; statistical analysis, L.B., R.L., H.L., Z.C.; and manuscript editing, L.B., R.L., W.F., H.Z., D.V., B.S., Z.C.

Funding:

This research was supported by the National Institutes of Health (grant 5R01 CA119053).

Conflicts of interest are listed at the end of this article.

See also Science to Practice in this issue.

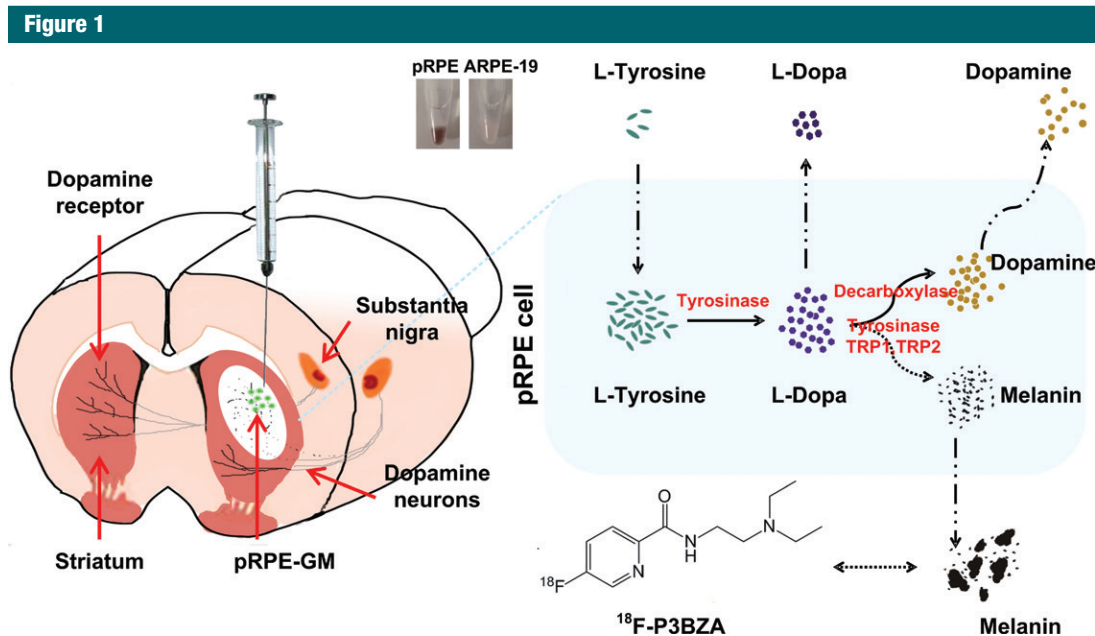


Figure 1: Schematic of ¹⁸F-P3BZA for imaging RPE cells in rat brains. Melanotic pRPE cells (shown in black in Eppendorf tube) attached to gelatin microcarriers (*pRPE-GM*), used as donor cells, and amelanotic ARPE-19 cells (shown in white in Eppendorf tube) attached to gelatin microcarriers (*ARPE-19-GM*) or gelatin microcarriers alone, used as controls, were implanted into left and right striatum, respectively, of normal rats.

Administrative Panel on Laboratory Animal Care at Stanford University. A schematic drawing of ¹⁸F-P3BZA for imaging of RPE cells in rat brains is shown in Figure 1. Details of methods are in Appendix E1 (online). This includes radiosynthesis of ¹⁸F-P3BZA (prepared according to a previously published procedure [21,22]). Melanotic pRPE (23) and amelanotic ARPE-19 cells (24) were used as positive and negative controls, respectively, for evaluating ¹⁸F-P3BZA in vitro and in vivo. pRPE cells were isolated according to a previously published procedure (25), which is also detailed in Appendix E1 (online).

In Vitro Assays

pRPE (generation 3) or control ARPE-19 cells (5×10^5) were plated in a 12-well plate pretreated with L-tyrosine (2 mmol/L) for 24 hours or not treated at all, followed by incubation with 74 kBq (2 μ Ci) per well of ¹⁸F-P3BZA at 37°C for 15, 30, 60, and 120 minutes. Here, L-tyrosine is one of the key substrates of the melanogenic pathway. It is typically used to boost melanin content in cells

and verify the specificity of melanin-targeted probes (26,27). The cells were washed three times with chilled phosphate-buffered saline and lysed with 500 μ L of 0.1 mol/L NaOH. The cell lysates were then collected and the radioactivity of the lysates was measured with a gamma counter (Perkin-Elmer, Waltham, Mass). The cell uptake was expressed as the percentage of total applied radioactivity. All experiments were performed with triplicate samples. Similarly, uptake of ¹⁸F-P3BZA at 30-minute incubation was determined in pRPE cells at different passages (passage numbers 3, 5, and 8, which are represented as pRPE-P3, pRPE-P5, and pRPE-P8, respectively) and control ARPE-19 cells, with or without pretreatment with L-tyrosine, to further evaluate the probe uptake characteristics for the pRPE cells during the passaging process.

In vitro measurement of melanin content was also performed for pRPE and ARPE-19 cells in parallel with the cell uptake assays according to methods reported previously (28).

Cell Implantation

RPE cells (pRPE and control ARPE-19 cells) were passively adsorbed or attached to gelatin microcarriers (Cytodex 1, 131–220- μ m diameter; GE Healthcare Life Sciences, Piscataway, NJ) according to typical methods (11). We illustrated the content of melanin in RPE cells by the unit of absorbance at 405 nm per milligram of protein, which is represented as A405 per milligram of protein.

Twenty-four female Wistar rats were used in this study. Melanotic pRPE or amelanotic ARPE-19 cells (approximately 12000–15000 cells in 10 μ L) were injected into striatum. The implantation procedure was performed following the surgical procedures described in a previous report (29).

PET/CT

Small-animal PET/CT was performed with a PET/CT system (Inveon; Siemens Healthcare Molecular Imaging, Knoxville, Tenn). For each rat, ¹⁸F-P3BZA (7.4 MBq, 200 μ Ci) was administered through the tail vein.

To assess the *in vivo* kinetics of ^{18}F -P3BZA in normal rat brain, a 70-minute dynamic PET scan was obtained in four normal rats. The results were divided by the injected dose (ID) to obtain an image region of interest–derived percentage of the ID per gram of tissue, and the time-activity curve was then calculated.

To evaluate the performance of ^{18}F -P3BZA for imaging implanted pRPE cells *in vivo*, static PET/CT was performed in normal rats by implanting pRPE cells or ARPE-19 cells attached to gelatin microcarriers ($n = 4$ for both) in the left striatum. Gelatin microcarriers alone were implanted in the right striatum as controls. PET/CT was performed 1 hour after tail vein injection of ^{18}F -P3BZA.

To evaluate the potential of ^{18}F -P3BZA for monitoring the survival and function of implanted RPE cells, longitudinal PET/CT scans were obtained 2, 9, and 16 days after cell implantation ($n = 12$). All live rats were imaged at each time point, and four rats were sacrificed after each PET/CT procedure. Thus, 12 rats were imaged on day 2, eight were imaged on day 9, and four were imaged on day 16. PET/CT image analysis was performed by radiologists B.S. and L.B. (with 28 and 13 years of experience, respectively).

Postmortem Analysis

Rats were sacrificed immediately after PET/CT, and rat brain slices were prepared for postmortem analysis. Because the spatial resolution and partial volume effects of PET may not allow for accurate determination of PET probe localization in specific brain regions, *ex vivo* autoradiography was performed. Immediately after static PET/CT, frozen axial brain slices (12 μm thick) were prepared for autoradiography. Quantitation of radioactivity in autoradiography images was performed by using Image J software (National Institutes of Health, Bethesda, Md). The brain slices adjacent to those for autoradiography study were stained with hematoxylin-eosin to identify the implantation sites and anatomy of brain sections.

To verify the presence of melanin, slices from the block containing a representative RPE cell profile on initial review were stained with Fontana-Masson stain after obtaining longitudinal PET/CT scans according to the manufacturer's recommendations. To identify the implanted pRPE cells, tissue slices adjacent to those for Fontana-Masson staining underwent immunohistochemistry staining with use of RPE65 (Chemicon, Temecula, Calif), following the manufacturer's recommendations. Postmortem analysis was performed by a neurologist (H.Z., with 19 years of experience).

Statistical Methods

Means were compared by using the Student *t* test, analysis of variance, and regression analysis. $P < .05$ was indicative of a significant difference. The Pearson correlation coefficients (R^2) were calculated to assess the relationship between ^{18}F -P3BZA cell uptake and melanin content in pRPE cells. Data were analyzed by using software (version 8.02; SAS Institute, Cary, NC).

Results

Synthesis of ^{18}F -P3BZA

High-performance liquid chromatography purification of ^{18}F -P3BZA yielded $9.5\% \pm 1.9$ radiochemical yields with 10.4-minute retention time, affording a product with more than 95% radiochemical purity and specific activity of 100–150 GBq/ μmol .

In Vitro Assays

Cell uptake results at multiple time points showed that ^{18}F -P3BZA accumulated effectively in pRPE cells but not in control ARPE-19 cells (Fig 2, A). The uptake of ^{18}F -P3BZA in pRPE cells maximized at a mean \pm standard deviation of $10.72\% \pm 0.38$ of applied activity within 30 minutes and remained at $9.09\% \pm 0.31$ and $8.61\% \pm 0.47$ at 60 and 120 minutes, respectively. At each time point, uptake in pRPE cells was significantly higher than that in the control ARPE-19 cells, which remained low ($P = .03$). For pRPE cells, there

was a pronounced increase in uptake for ^{18}F -P3BZA after treatment with tyrosine, which was approximately three- to fourfold higher than that in nontreatment groups. For the control ARPE-19 cells, however, there was no difference before and after tyrosine treatment ($P = .25$).

The cell uptake of ^{18}F -P3BZA in pRPE cells at different passages showed that pRPE-P3 had the greatest uptake, followed by pRPE-P5 and then pRPE-P8 (the decreasing rate is -1.45% of applied activity per passage, $P < .0001$), with a decreasing response to tyrosine treatment. After tyrosine treatment, uptake of ^{18}F -P3BZA in pRPE-P3, pRPE-P5, and pRPE-P8 was increased by 48.8%, 37.8%, and 31.9%, respectively (Fig 2, B). There was no difference for the probe uptake between L-tyrosine–treated ARPE-19 cells and untreated ARPE-19 cells ($P = .13$).

The amount of ^{18}F -P3BZA uptake (mean, $10.71\% \pm 0.38$, $6.25\% \pm 0.59$, $3.29\% \pm 0.15$, and $1.31\% \pm 0.15$ of applied activity) was highly correlated with the melanin content (14.34 A405 per milligram of protein ± 0.48 , 7.71 A405 per milligram of protein ± 0.50 , 6.04 A405 per milligram of protein ± 0.38 , and 5.56 A405 per milligram of protein ± 0.21) in pRPE cells and control ARPE-19 cells (Fig 2, C, $R^2 = 0.91$). Melanogenesis was reduced with an increasing number of pRPE cell passages (rate of decrease, -1.57 A405 per milligram of protein per passage; $P = .0011$) (Fig 2, D).

Dynamic PET Scans in Normal Rat Brain

Dynamic PET images provided visual evidence that ^{18}F -P3BZA could rapidly cross the blood-brain barrier and accumulate in the brain. Moreover, most of the probe was cleared at 28 minutes after injection (Fig 3, A). Similarly, the time-activity curve of brain from dynamic PET scans demonstrated that ^{18}F -P3BZA rapidly accumulated in the rat brain (Fig 3, B), peaked at $7.61\% \text{ ID/g} \pm 0.30$ within the first 2 minutes, and then gradually decreased over the remaining scanning time. The amount of ^{18}F -P3BZA

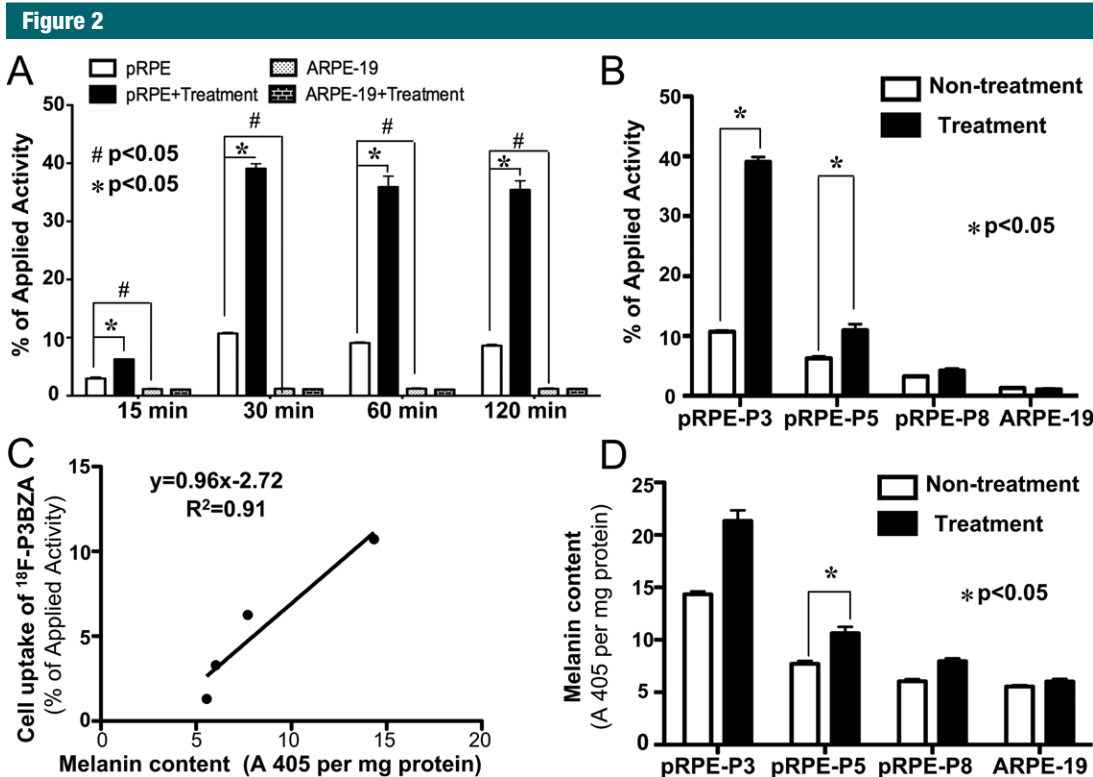


Figure 2: In vitro cell uptake of ¹⁸F-P3BZA and quantification analysis of melanin. *A*, Bar chart shows time-dependent uptake of ¹⁸F-P3BZA after incubation for 15, 30, 60, or 120 minutes in pRPE cells and control ARPE-19 cells, with or without pretreatment with tyrosine for 24 hours. Results are means of triplicate measurements ± standard deviations. *B*, Bar chart shows uptake of ¹⁸F-P3BZA after 30 minutes of incubation in pRPE cells of different passage numbers and control ARPE-19 cells with or without pretreatment with tyrosine. Results are means of triplicate measurements ± standard deviations. *C*, Graph shows correlation between uptake of ¹⁸F-P3BZA and melanin content at different passage numbers of pRPE cells and control ARPE-19 cells. *D*, Bar chart shows results of quantification analysis of melanin for pRPE cells of different passage numbers and control ARPE-19 cells with or without tyrosine incubation for 24 hours ($n = 4$). Data are means ± standard deviations.

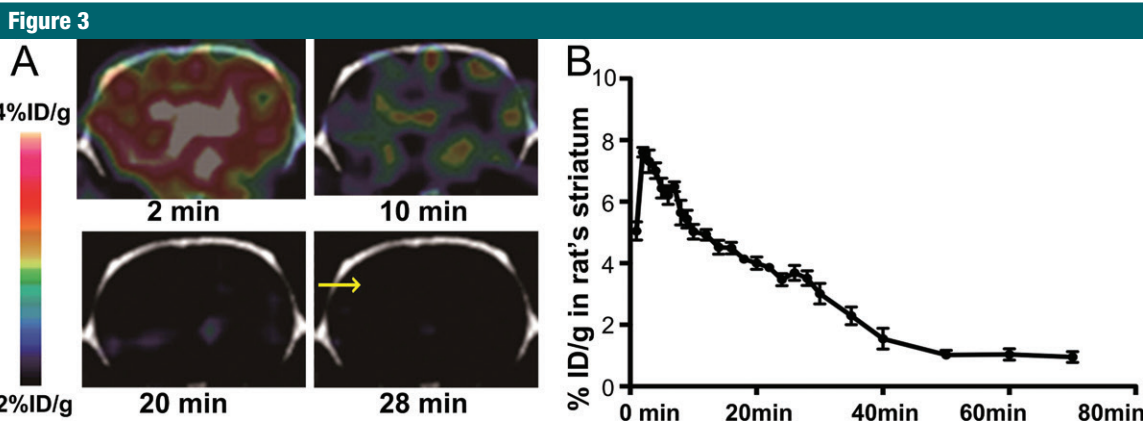


Figure 3: Images from in vivo dynamic PET of ¹⁸F-P3BZA in normal rat brain. *A*, Representative decay-corrected coronal images of normal rat brain. Arrow shows brain PET/CT image 28 minutes after injection of ¹⁸F-P3BZA. *B*, Time-activity curve derived from PET studies in normal rat brain across striatum level. Results are expressed as percentage of ID per gram of brain tissue ± standard deviation ($n = 4$).

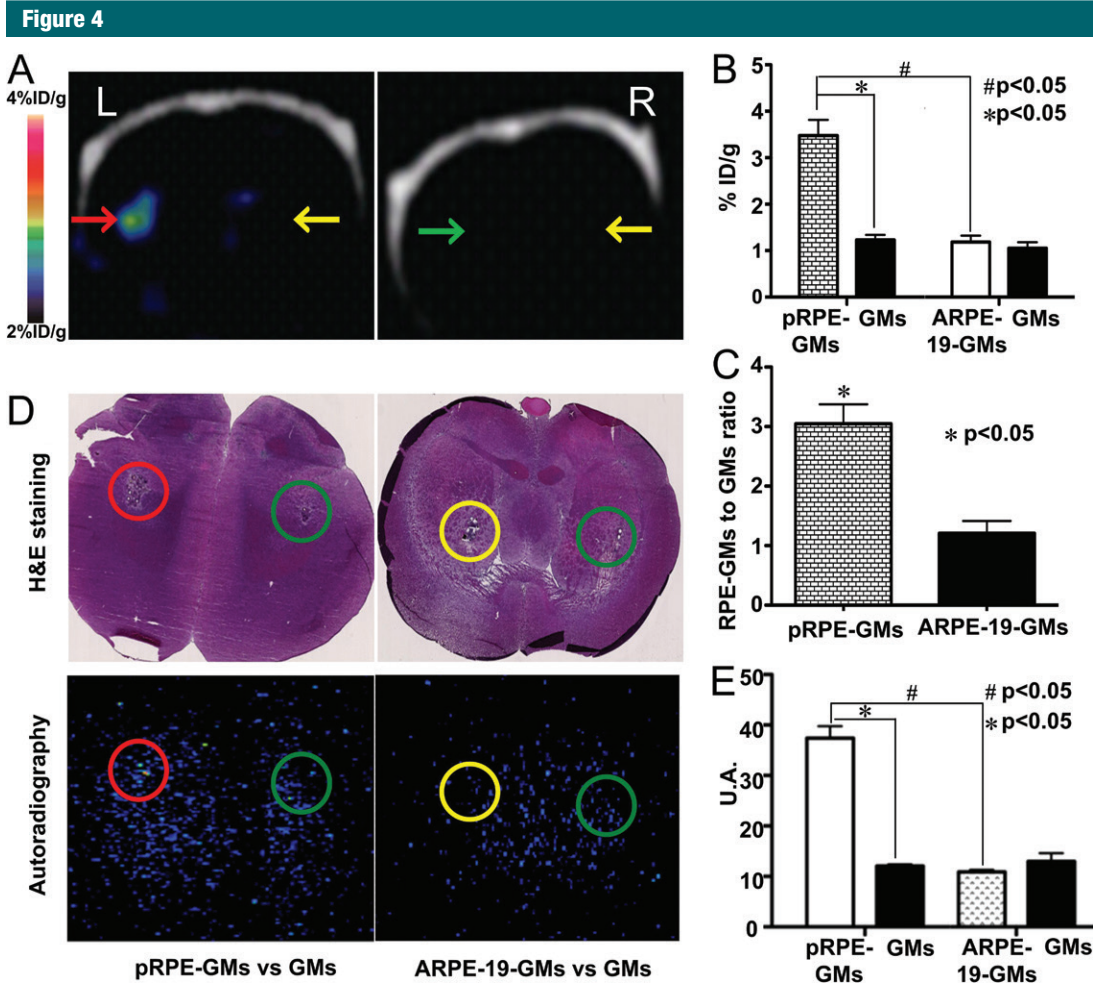


Figure 4: In vivo static PET/CT images of ^{18}F -P3BZA 2 days after cell implantation. *A*, Representative decay-corrected coronal PET/CT images after implantation of gelatin microcarrier-bound pRPE cells (red arrow). Gelatin microcarrier-bound ARPE-19 cells (green arrow) and gelatin microcarrier alone (yellow arrows) were used as controls. *B*, Bar chart shows results of quantitative analysis of small animal coronal PET images for uptake of ^{18}F -P3BZA. The signal of gelatin microcarrier-bound pRPE cells (*pRPE-GMs*) is much higher than that of gelatin microcarrier-bound ARPE-19 cells or gelatin microcarriers alone. Results are expressed as percentage of ID per gram of brain tissue \pm standard deviation. There were four animals in each group. *C*, Bar chart shows gelatin microcarrier-bound RPE cell-to-gelatin microcarrier uptake ratios for gelatin microcarrier-bound pRPE cells (*pRPE-GMs*) and gelatin microcarrier-bound ARPE-19 cells (*ARPE-GMs*). *D*, Representative hematoxylin-eosin (H&E)-stained and coronal autoradiography images. The combination of autoradiography and hematoxylin-eosin staining further demonstrates that ^{18}F -P3BZA uptake in gelatin microcarrier-bound pRPE cells (*pRPE-GMs*) is much higher than that in either gelatin microcarrier-bound ARPE-19 cells (*ARPE-19-GMs*) or gelatin microcarriers (*GMs*) alone. Green circles = implantation sites for gelatin microcarriers, red circles = implantation sites for gelatin microcarrier-bound pRPE cells, yellow circles = implantation sites for gelatin microcarrier-bound ARPE-19 cells. *E*, Bar chart shows results of quantitative analysis of autoradiography images processed with Image J software. *pRPE-GMs* = gelatin microcarrier-bound pRPE cells, *GMs* = gelatin microcarriers, *ARPE-19-GMs* = gelatin microcarrier-bound ARPE-19 cells. Results of radioactivity in autoradiography images are expressed as brightness in circle. Value of brightness is generated with Image J software. U.A. = arbitrary units.

accumulated in brain decreased to 3.54% ID/g \pm 0.21 at 28 minutes after injection and further decreased to 1.04% ID/g \pm 0.37 at 60 minutes after injection (rate of decrease, -0.16% ID/g/min; $P < .0001$).

In Vivo Small-Animal Static PET/CT, ex Vivo Autoradiography, and Hematoxylin-Eosin Staining

On PET/CT scans, the injected microcarrier-bound pRPE cells were clearly visualized with high contrast, whereas

both control gelatin microcarrier-bound ARPE-19 cells and the contralateral control gelatin microcarriers could not be delineated (Fig 4, A). Results of quantification analysis are summarized in Figure 4, B. The uptake of

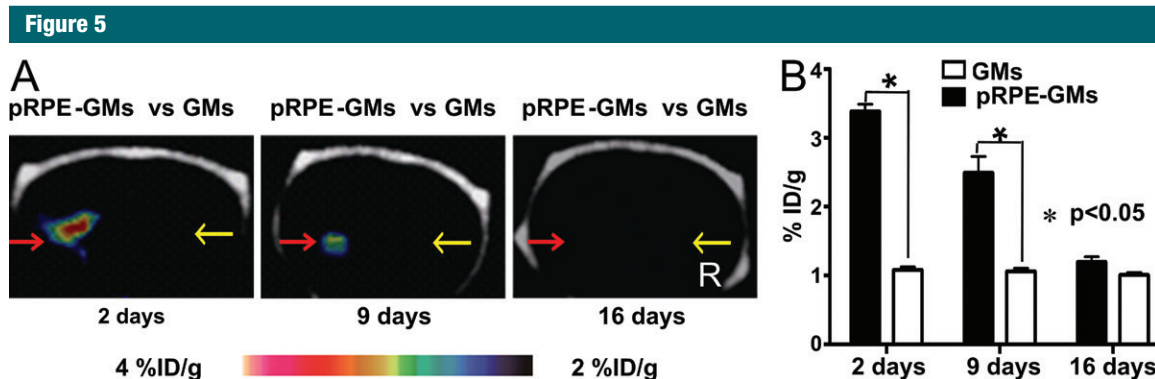


Figure 5: Images from longitudinal ¹⁸F-P3BZA PET/CT performed 2, 9, and 16 days after implantation of gelatin microcarrier-bound pRPE cells (pRPE-GMs) in normal rats. *A*, Representative decay-corrected longitudinal PET/CT images. Red arrows = implantation sites for gelatin microcarrier-bound pRPE cells, yellow arrows = implantation sites for gelatin microcarriers (GMs). *B*, Bar chart shows results of quantification analysis of longitudinal ¹⁸F-P3BZA PET/CT. Results are means \pm standard deviations. Four rats were evaluated at each time point.

¹⁸F-P3BZA in gelatin microcarrier-bound pRPE cells (mean, 3.48% ID/g \pm 0.58) was higher than that in control microcarrier-bound ARPE-19 cells or gelatin microcarriers alone (1.23% ID/g \pm 0.19 and 1.19% ID/g \pm 0.23, respectively; $P = .003$). The gelatin microcarrier-bound pRPE cell-to-control gelatin microcarriers uptake ratio was significantly higher than the gelatin microcarrier-bound ARPE-19 cell-to-gelatin microcarriers uptake ratio (mean, 3.05 \pm 0.57 vs 1.21 \pm 0.36, respectively; $P = .04$) (Fig 4, C).

The implantation sites and the anatomy of brain sections were easily recognized (Fig 4, D). All of the cells and gelatin microcarriers injected were within the striatum and formed clumps.

Autoradiography images also revealed prominent ¹⁸F-P3BZA accumulation in the area of the gelatin microcarrier-bound pRPE cell transplant site. A "hot spot" was evident in the region that exhibited both microcarrier aggregation and structural changes due to surgery in the parallel macroscopic hematoxylin-eosin-stained section. No visible hot spot could be identified in the injection sites for control gelatin microcarrier-bound RPE-19 cells or contralateral gelatin microcarriers alone. Results of quantitative analysis showed that the signal of the transplant site for the gelatin microcarrier-bound pRPE cells was significantly higher than that of injection sites for gelatin

microcarrier-bound ARPE-19 cells or contralateral gelatin microcarriers alone ($P < .0001$) (Fig 4, E).

Longitudinal PET/CT Scans

PET/CT demonstrated that ¹⁸F-P3BZA accumulation in gelatin microcarrier-bound pRPE cells decreased gradually with time after implantation (Fig 5). The gelatin microcarrier-bound pRPE cells were visible as a strong hot spot 2 days after implantation, whereas the imaging signal of gelatin microcarrier-bound pRPE cells was much weaker and was visible as a moderate hot spot 9 days after implantation. At 16 days, hot spots could not be clearly recognized. Uptake of ¹⁸F-P3BZA peaked at 3.39% ID/g \pm 0.18 at 2 days after implantation, then decreased to 2.49% ID/g \pm 0.41 at 9 days and dropped to a baseline level (1.20% ID/g \pm 0.13) at 16 days (rate of decrease, -0.16% ID/g per day; $P < .0001$).

Fontana-Masson Staining and Immunohistochemistry Staining

RPE65-positive cells were found to surround the gelatin microcarriers closely at days 2, 9, and 16 (Fig 6). Melanin was identified as black spots by means of Fontana-Masson staining. At day 2, we observed a lot of granular melanin spots both inside and outside of pRPE cells. A moderate amount of spots were seen at day 9, and a very small number of spots were seen at day 16.

Discussion

¹⁸F-P3BZA can be easily prepared by means of one-step radiosynthesis. It displays high melanin targeting specificity and shows excellent performance for in vivo imaging of melanotic melanoma (21,22). In our study, as expected, ¹⁸F-P3BZA specifically and effectively localizes in pRPE cells in a melanin-dependent manner in vitro and in vivo. In vitro, correlation analysis demonstrated a strong correlation between the uptake of ¹⁸F-P3BZA and the melanin content in pRPE cells. Our in vivo PET imaging study of rats implanted with cells showed that ¹⁸F-P3BZA could help clearly delineate the implanted pRPE cells from the background brain signal, but not ARPE19-gelatin microcarriers or gelatin microcarriers, at 2 days after implantation. This finding was further confirmed with autoradiography and hematoxylin-eosin staining, which showed subjective similar locations of the ¹⁸F-P3BZA in the expected region of RPE cells transplanted into the striatum.

Our study also revealed that PET with ¹⁸F-P3BZA provides excellent imaging contrast. High gelatin microcarrier-bound pRPE cell-to-contralateral gelatin microcarrier or adjacent normal striatum uptake ratios can be obtained (3.05 \pm 0.57 and 3.19 \pm 0.53, respectively). These high ratios are mainly attributed to the high melanin

Figure 6

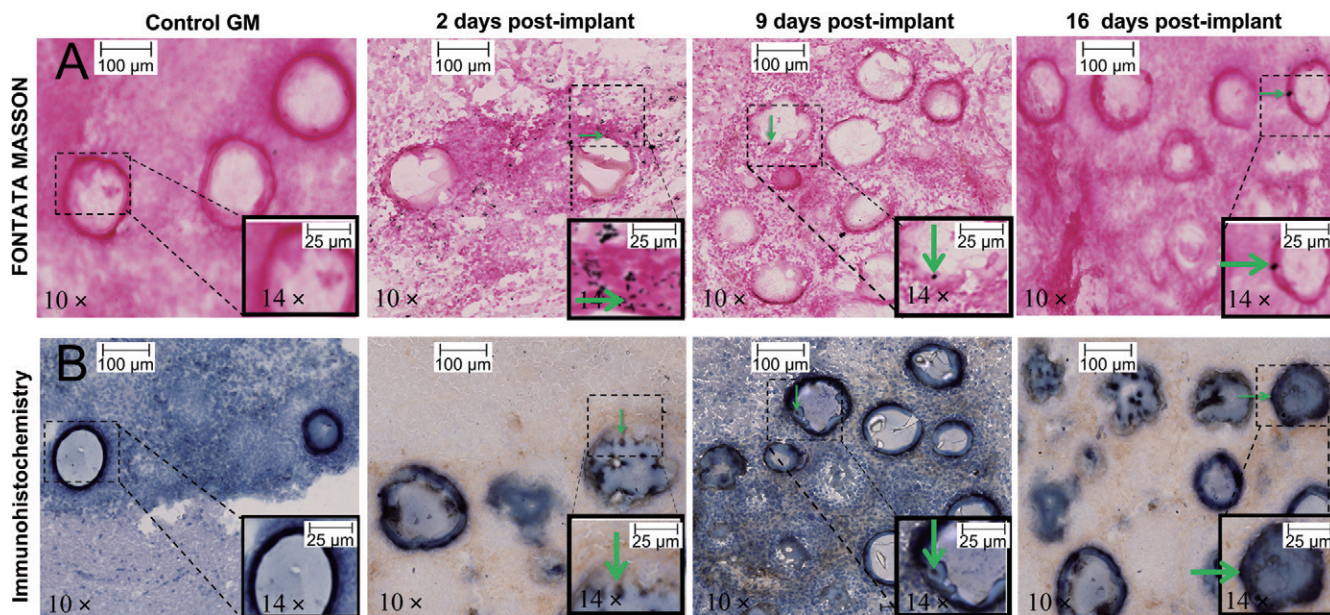


Figure 6: Representative photomicrographs of rat brain slices stained with Fontana-Masson and immunohistochemistry stains. Rats with intrastriatal implantation of control gelatin microcarriers (*GM*) and gelatin microcarrier-bound pRPE cells were sacrificed 2, 9, and 16 days after implantation and brain tissues were sliced and stained. With immunohistochemistry staining, pRPE cells were characterized as positive for RPE-65 and adhered onto surface of gelatin microcarriers. Fontana-Masson staining shows melanin as black pigmentations in granular or cluster shapes. On photomicrographs obtained with Fontana-Masson stain, nucleus is stained red with nuclear fast red. Green arrows indicate representative pRPE cells with matched melanin presented inside or outside.

targeting specificity of ^{18}F -P3BZA as well as the lack of endogenous melanin in striatum area (30). Considering that the RPE cells are only implanted into the striatum of patients, a high RPE cell uptake of ^{18}F -P3BZA to striatum ratio is expected in humans. This is a major advantage of ^{18}F -P3BZA over other PET probes such as the previously reported carbon 11 (^{11}C)-raclopride or ^{18}F -fluoro-L-DOPA (31–33). For these two probes, the endogenous dopamine or enzymatic activities could compromise their performance in the imaging of implanted RPE cells, and the imaging quality of these two probes is quite poor. For example, before and after implantation of the RPE cells, the implantation site (striatum)-to-cortex uptake ratios were only 1.35 ± 0.10 and 1.48 ± 0.07 for ^{18}F -fluoro-L-DOPA and 2.41 ± 0.74 and 2.44 ± 0.67 , respectively, for ^{11}C -raclopride (32). More important, ^{11}C -raclopride and ^{18}F -fluoro-L-DOPA PET display the overall information from endogenous

dopamine release or enzymatic activities and the changes caused by implanted RPE cells. Thus, it is difficult to use them for evaluating the treatment efficacy of RPE cells.

In our study, longitudinal PET/CT scans showed a significant reduction in uptake of ^{18}F -P3BZA in the gelatin microcarrier-bound pRPE cells over time, suggesting the reduction of the total melanogenesis in implanted cells. Results of immunohistochemistry staining demonstrated that an appreciable number of implanted pRPE cells survived over the 16-day experimental period, with the number of cells only slightly reduced. This result is consistent with those from other reports (11,12,34). However, results of Fontana-Masson staining revealed that the amount of melanin decreases sharply over time. Therefore, it is likely that the diminished uptake of ^{18}F -P3BZA is caused mainly by the reduced activity of melanin synthesis in pRPE cells as cells divide. Our in vitro results provide evidence to support

this explanation. Indeed, as pRPE cell passages advance, melanin content decreases and the uptake of ^{18}F -P3BZA decreases accordingly.

Because the activity of the melanin synthesis pathway provides a rationale for the application of hRPE cells in Parkinson disease therapy, the source of hRPE donor cells is crucial for successful therapy. However, melanogenesis in adult RPE cells remains controversial. Some scientists believe that melanin synthesis occurs in hRPE cells throughout a person's life, albeit at a slow rate, whereas others consider that it ceases at birth (8,35). Age-related change of melanin expression in hRPE cells has thus been studied (36). In our study, we adopted adult pRPE cells as the source of donor cells, and this may explain part of the diminished activity of ^{18}F -P3BZA over time. Similarly, most previous reports of hRPE cell therapy for Parkinson disease did not define standard criteria for the selection of donor cells. Therefore, the use of cells obtained from

donors of different ages may be partly responsible for the variation and inconsistencies in the treatment outcomes from different clinical trials.

Some limitations in our study should be noted. ^{18}F -P3BZA PET cannot help differentiate the melanin loss caused by either poor cell survival or low melaninogenesis activity. However, this limitation is not likely to be an issue because both poor cell survival and low melaninogenesis activity can reduce treatment efficacy. A second limitation is that our study is based on a rat model with porcine RPE cells as the source of donor cells. It is necessary to further study the efficacy of ^{18}F -P3BZA PET in humans or nonhuman primates by using allograft hRPE cells.

Practical applications: ^{18}F -P3BZA PET/CT is a feasible technique for visualizing and detecting the long-term activity of implanted RPE cells for the treatment of Parkinson disease in vivo. ^{18}F -P3BZA PET/CT provides opportunities to visualize, characterize, and detect the long-term activity of implanted RPE cells. Practical applications lie in the possibility of improving the therapeutic efficacy of hRPE cells for Parkinson disease treatment in the clinic.

Acknowledgment: The authors thank Lijun Xu, MD, from the Department of Anesthesia of Stanford University School of Medicine for technical support.

Disclosures of Conflicts of Interest: **L.B.** Financial activities related to the present article: none to disclose. Financial activities not related to the present article: none to disclose. Other relationships: has a patent pending. **R.L.** No relevant conflicts of interest to disclose. **H.L.** No relevant conflicts of interest to disclose. **W.F.** No relevant conflicts of interest to disclose. **X.X.** No relevant conflicts of interest to disclose. **H.Z.** No relevant conflicts of interest to disclose. **D.V.** No relevant conflicts of interest to disclose. **B.S.** No relevant conflicts of interest to disclose. **Z.C.** Financial activities related to the present article: none to disclose. Financial activities not related to the present article: none to disclose. Other relationships: has a patent pending.

References

- de Lau LM, Breteler MM. Epidemiology of Parkinson's disease. *Lancet Neurol* 2006; 5(6):525–535.
- Olanow CW. Levodopa/dopamine replacement strategies in Parkinson's disease—future directions. *Mov Disord* 2008;23(Suppl 3):S613–S622.
- Poewe W, Mahlknecht P, Jankovic J. Emerging therapies for Parkinson's disease. *Curr Opin Neurol* 2012;25(4):448–459.
- Olanow CW, Obeso JA, Stocchi F. Continuous dopamine-receptor treatment of Parkinson's disease: scientific rationale and clinical implications. *Lancet Neurol* 2006;5(8):677–687.
- Hayes MW, Fung VS, Kimber TE, O'Sullivan JD. Current concepts in the management of Parkinson disease. *Med J Aust* 2010;192(3):144–149.
- Roffler-Tarlov S, Liu JH, Naumova EN, Bernal-Ayala MM, Mason CA. L-Dopa and the albino riddle: content of L-Dopa in the developing retina of pigmented and albino mice. *PLoS ONE* 2013;8(3):e57184.
- Tombran-Tink J, Shivaram SM, Chader GJ, Johnson LV, Bok D. Expression, secretion, and age-related downregulation of pigment epithelium-derived factor, a serpin with neurotrophic activity. *J Neurosci* 1995;15(7 Pt 1):4992–5003.
- Schraermeyer U, Kopitz J, Peters S, et al. Tyrosinase biosynthesis in adult mammalian retinal pigment epithelial cells. *Exp Eye Res* 2006;83(2):315–321.
- Dorey CK, Torres X, Swart T. Evidence of melanogenesis in porcine retinal pigment epithelial cells in vitro. *Exp Eye Res* 1990;50(1):1–10.
- Kubrusly RC, Guimarães MZ, Vieira AP, et al. L-DOPA supply to the neuro retina activates dopaminergic communication at the early stages of embryonic development. *J Neurochem* 2003;86(1):45–54.
- Flores J, Cepeda IL, Cornfeldt ML, O'Kusky JR, Doudet DJ. Characterization and survival of long-term implants of human retinal pigment epithelial cells attached to gelatin microcarriers in a model of Parkinson disease. *J Neuroopathol Exp Neurol* 2007;66(7):585–596.
- Subramanian T, Marchionini D, Potter EM, Cornfeldt ML. Striatal xenotransplantation of human retinal pigment epithelial cells attached to microcarriers in hemiparkinsonian rats ameliorates behavioral deficits without provoking a host immune response. *Cell Transplant* 2002;11(3):207–214.
- Watts RL, Raiser CD, Stover NP, et al. Stereotaxic intrastriatal implantation of human retinal pigment epithelial (hRPE) cells attached to gelatin microcarriers: a potential new cell therapy for Parkinson's disease. *J Neural Transm Suppl* 2003(65):215–227.
- Stover NP, Bakay RA, Subramanian T, et al. Intrastratial implantation of human retinal pigment epithelial cells attached to microcarriers in advanced Parkinson disease. *Arch Neurol* 2005;62(12):1833–1837.
- Stover NP, Watts RL. Spheramine for treatment of Parkinson's disease. *Neurotherapeutics* 2008;5(2):252–259.
- Gross RE, Watts RL, Hauser RA, et al. Intrastratial transplantation of microcarrier-bound human retinal pigment epithelial cells versus sham surgery in patients with advanced Parkinson's disease: a double-blind, randomised, controlled trial. *Lancet Neurol* 2011;10(6):509–519.
- Cenci MA, Widner H. Parkinson disease: poor results for retinal cell transplants in Parkinson disease. *Nat Rev Neurol* 2011;7(8):424–425.
- Albanese A. Cell therapy for Parkinson's disease: have the glory days gone? *Lancet Neurol* 2011;10(6):492–493.
- McKay BS, Goodman B, Falk T, Sherman SJ. Retinal pigment epithelial cell transplantation could provide trophic support in Parkinson's disease: results from an in vitro model system. *Exp Neurol* 2006;201(1):234–243.
- Zareba M, Raciti MW, Henry MM, Sarna T, Burke JM. Oxidative stress in ARPE-19 cultures: do melanosomes confer cytoprotection? *Free Radic Biol Med* 2006;40(1):87–100.
- Liu H, Liu S, Miao Z, et al. Development of ^{18}F -labeled picolinamide probes for PET imaging of malignant melanoma. *J Med Chem* 2013;56(3):895–901.
- Qin C, Cheng K, Chen K, et al. Tyrosinase as a multifunctional reporter gene for photoacoustic/MRI/PET triple modality molecular imaging. *Sci Rep* 2013;3:1490.
- Zhang HL, Wu JJ, Ren HM, Wang J, Su YR, Jiang YP. Therapeutic effect of microencapsulated porcine retinal pigmented epithelial cells transplantation on rat model of Parkinson's disease. *Neurosci Bull* 2007;23(3):137–144.
- Dunn KC, Aotaki-Keen AE, Putkey FR, Hjelmeland LM. ARPE-19, a human retinal pigment epithelial cell line with differentiated properties. *Exp Eye Res* 1996;62(2):155–169.
- Feng W, Yasumura D, Matthes MT, LaVail MM, Vollrath D. Merck triggers uptake of photoreceptor outer segments during phagocytosis by cultured retinal pigment epithelial cells. *J Biol Chem* 2002;277(19):17016–17022.

26. Kim HJ, Kim DY, Park JH, et al. Synthesis and characterization of a (68)Ga-labeled N-(2-diethylaminoethyl)benzamide derivative as potential PET probe for malignant melanoma. *Bioorg Med Chem* 2012;20(16):4915–4920.
27. Ren G, Miao Z, Liu H, et al. Melanin-targeted preclinical PET imaging of melanoma metastasis. *J Nucl Med* 2009;50(10):1692–1699.
28. Ishikawa M, Kawase I, Ishii F. Glycine inhibits melanogenesis in vitro and causes hypopigmentation in vivo. *Biol Pharm Bull* 2007;30(11):2031–2036.
29. Cepeda IL, Flores J, Cornfeldt ML, O'Kusky JR, Doudet DJ. Human retinal pigment epithelial cell implants ameliorate motor deficits in two rat models of Parkinson disease. *J Neuropathol Exp Neurol* 2007;66(7):576–584.
30. Fedorow H, Tribl F, Halliday G, Gerlach M, Riederer P, Double KL. Neuromelanin in human dopamine neurons: comparison with peripheral melanins and relevance to Parkinson's disease. *Prog Neurobiol* 2005;75(2):109–124.
31. Wang R, Zhang J, Guo Z, et al. In-vivo PET imaging of implanted human retinal pigment epithelium cells in a Parkinson's disease rat model. *Nucl Med Commun* 2008;29(5):455–461.
32. Doudet DJ, Cornfeldt ML, Honey CR, Schweikert AW, Allen RC. PET imaging of implanted human retinal pigment epithelial cells in the MPTP-induced primate model of Parkinson's disease. *Exp Neurol* 2004;189(2):361–368.
33. Yin F, Tian ZM, Liu S, et al. Transplantation of human retinal pigment epithelium cells in the treatment for Parkinson disease. *CNS Neurosci Ther* 2012;18(12):1012–1020.
34. Farag ES, Vinters HV, Bronstein J. Pathologic findings in retinal pigment epithelial cell implantation for Parkinson disease. *Neurology* 2009;73(14):1095–1102.
35. Schraermeyer U. Does melanin turnover occur in the eyes of adult vertebrates? *Pigment Cell Res* 1993;6(4 Pt 1):193–204.
36. Sarna T, Burke JM, Korytowski W, et al. Loss of melanin from human RPE with aging: possible role of melanin photooxidation. *Exp Eye Res* 2003;76(1):89–98.